DOI: 10.1002/ejic.201000204

# Organic-Additive-Assisted Synthesis of Hierarchically Meso-/Macroporous Titanium Phosphonates

Tian-Yi Ma[a] and Zhong-Yong Yuan*[a]

**Keywords:** Organic-inorganic hybrid composites / Titanium / Phosphonates / Adsorption / Mesoporous materials

Organic-inorganic hybrid materials of meso-/macroporous titanium triphosphonate materials were synthesized by using amino tri(methylene phosphonic acid) as the coupling molecule. The preparation was accomplished by a hydrothermal process in the presence or absence of small amounts of the diblock copolymer $EO_{30}PO_{34}$ and β-cyclodextrin as the organic additives. The organic-additive-assisted preparation efficiently aided the enlargement of the surface areas and pore volumes of the resultant porous titanium triphosphonates and helped improve the wormhole-like mesoporosity. In addition to the large macrochannels, with a size of 500–1000 nm, observed in all the titanium phosphonates synthesized with or without organic additives, a secondary small-scaled, spherical macroporous structure with a diameter of 50–100 nm was obtained by the addition of cyclodextrin. These macroporous structures are proposed to be templated by the aggregation of cyclodextrin. The structural characterization confirms the integrity of organic groups inside the framework. Large adsorption capacities for heavy metal ions and $CO_2$ are demonstrated in these hybrid materials, which makes them promising adsorbents for practical applications.

## Introduction

Porous metal phosphonate materials have recently attracted increasing research interest because of their potential applications as sorbents, ion exchangers, ionic conductors, and catalysts.[1–3] The great variety of organophosphorus acids and their derivatives (salts, esters) also allows the rational design and control of the porous architecture of the resultant metal phosphonates as well as of the physicochemical properties in the area of optical behavior, catalysis, adsorption ability, etc.[4–6] A large number of metal phosphonate compounds have been synthesized by different methods and strategies,[7–11] in which the organic component can be varied and their microporous structures may be constructed by the stacking of the metal–organic phosphonate layers. The use of multidentate building blocks, such as amino-bridged tetraphosphonate groups,[1] has recently been found to render the formation of novel zirconium polyphosphonate open-framework compounds with a modular structure, and the dimensions of the cavities/channels inside the structures may be tailored by the right choice of the interlinking organic groups. By using terminal $RPO_3$ substituting groups, mesoporous metal phosphate/phosphonate materials were synthesized,[12,13] but the incorporation of phosphonate into the final materials is limited and mostly restricted to the pore surface. Organically bridged diphosphonic acids [$(HO)_2OP\text{-}R\text{-}PO(OH)_2$] with limited types of alkylene-bridging groups were then used to prepare mesoporous aluminum diphosphonates,[14–18] but their possible applications have not yet been reported. Periodic mesoporous[19] and macroporous[20] hydroxyethylidene-bridged titanium diphosphonate materials were recently synthesized for practical applications.

Many efforts have been made towards the incorporation of macropores in mesoporous materials by various means,[21] and it has been demonstrated that hierarchically nanoporous materials with channel-like macrostructures could be formed by a spontaneous assembly process in the absence/presence of surfactant molecules.[22,23] It was found that the addition of some organic additives influenced the textural properties and porosity of the resultant solids.[24] Materials with hierarchically meso-/macropores have enhanced properties relative to those of single-sized porous materials because of increased mass transport and reduced diffusion resistance through the material and the maintenance of a specific surface area on the level of fine pore systems.[21] For example, superior photocatalytic activity has been observed in hierarchically meso-/macroporous titanias because of the light-harvesting macroporous channels,[25] and metal phosphonates[26,27] and oxide–phosphonate hybrids[28,29] with porous hierarchy have exhibited enhanced catalytic activity and adsorption capacity. In this work, we describe a simple strategy for the preparation of titanium phosphonate materials with a hierarchically

[a] Institute of New Catalytic Materials Science, Key Laboratory of Energy-Material Chemistry (Tianjin) & Engineering Research Center of Energy Storage and Conversion (Ministry of Education), College of Chemistry, Nankai University, Tianjin 300071, China
Fax: +86-22-23509610
E-mail: zyyuan@nankai.edu.cn

Supporting information for this article is available on the WWW under http://dx.doi.org/10.1002/ejic.201000204.

  

meso-/macroporous structure, constructed with an amino-bridged alkylenephosphonic acid as the coupling molecule. The preparation process was carried out in the absence and presence of the organic additive diblock copolymer $EO_{30}PO_{34}$ and β-cyclodextrin. Because of the different organic additives used, the hierarchically porous structure and the adsorption abilities for heavy metal ions and $CO_2$ were distinct, which demonstrate the possibility of a purposive adjustment at the molecule level.

## Results

### Material Synthesis and Characterization

The synthesis of hierarchically meso-/macroporous amino-bridged titanium triphosphonate materials was performed by hydrolysis of tetrabutyl titanate in the phosphonic acid solution [amino tri(methylene phosphonic acid), ATMP; pH < 1] in the presence or absence of the block copolymer $EO_{30}PO_{34}$ and β-cyclodextrin as the organic additives, followed by autoclaving at 80 °C for 24 h. Removal of $EO_{30}PO_{34}$ and β-cyclodextrin was accomplished by extraction with ethanol solution at a relatively low temperature for the protection of the organophosphonate framework.

Figure 1 shows the representative SEM images of the obtained samples, which reveals macroporous structures in all the samples synthesized with and without organic additive assistance (sample prepared in the presence of $EO_{30}PO_{34}$ only: A-poly; prepared in the presence of β-CD only: A-CD; prepared in the absence of organic additives: A-non). The macropores have a channel-like shape with a uniform distribution and diameters in the range 500–1000 nm. They mostly have a one-dimensional orientation, parallel to each other, and are perforative through almost the entire particle. The macroporous framework is composed by the assembly of these small particles. This framework is quite similar to those of previously reported surfactant-assisted meso-/macrostructured metal oxide materials.[30,31] Moreover, careful examination of these SEM micrographs reveals that the pore wall of the large macropores in A-CD are separated by smaller spherical pores with the size of 50–100 nm, which thereby forms a two-scaled macroporous structure (Figure 1e). It is reminiscent of the hierarchically meso-/macroporous titanium phosphates synthesized in the presence of the polyethylene oxide surfactant Brij 56,[32] which indicates that the surfactant molecules are not necessary for the formation of the macrochannels, but the addition of a small amount of β-cyclodextrin could lead to the presence of secondary small-scaled macropores. The TEM images present a particulate morphology between the macrochannels of the samples (Figure 2).

An ill-defined mesostructure could be seen in the sample A-non (Figure 2a), which is composed of interconnected titanium phosphonate particles that were the hydrolysis product of tetrabutyl titanate in the phosphonic acid solution. Because of the addition of diblock copolymer $EO_{30}PO_{34}$, the sample (A-poly) exhibits well-structured

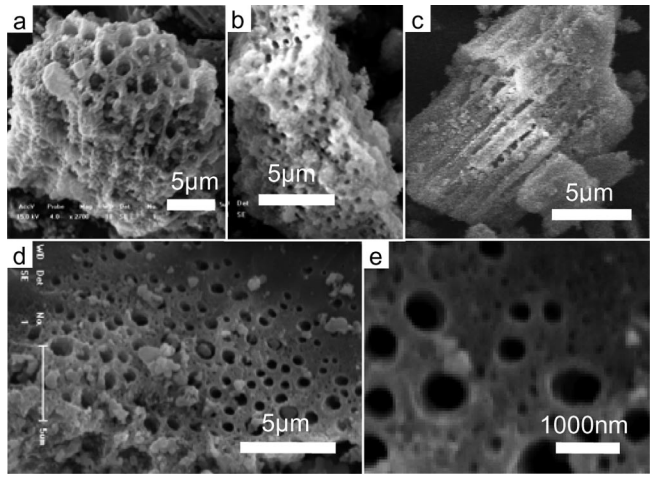


Figure 1. SEM images of (a) A-non, (b, c) A-poly and (d, e) A-CD.

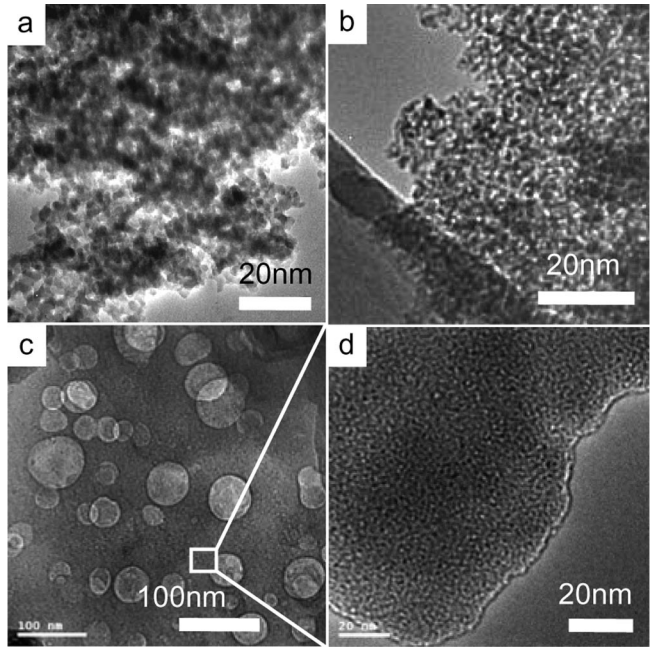


Figure 2. TEM images of (a) A-non, (b) A-poly and (c, d) A-CD.

wormhole-like mesopores (Figure 2b), which are aggregated by much smaller nanoparticles than those of A-non. While in the sample A-CD, synthesized in the presence of β-cyclodextrin, spherical pores with diameters of 50–100 nm are observed (Figure 2c), which correspond to the secondary macropores in the SEM images, and the walls between them are of wormhole-like mesostructure (Figure 2d). The nearly spherical cyclodextrin aggregates with diameters of about 100 nm are reported to present at lower concentrations,[33] which act as inverse templates to the spherical pores herein. The observed wormhole-like mesoporous structures between the spherical pores are very similar to the mesoporous silica materials templated by cyclodextrins.[34]

The nitrogen sorption isotherms and the corresponding pore size distributions calculated by BJH and NLDFT methods of A-non, A-poly, and A-CD are shown in Fig-

  

ure 3; their textural properties are listed in Table 1. The isotherm of A-non is of type II with no adsorption–desorption hysteresis, and the amount adsorbed increases gradually as the relative pressure increases, which was reported for the adsorption on some macroporous solids,[35] consistent with the SEM observations. The isotherms of A-poly and A-CD are of type IV rather than of type II, characteristic of mesoporous materials.[35] The hysteresis loops do not level off at the relative pressures close to the saturation vapor pressure, which is indicative of type H3 hysteresis; this suggests that the materials comprise aggregates (loose assemblages) of particles forming slitlike pores.[35] The corresponding BJH pore size distribution curve of A-non shows a wide peak around 1.8 nm (Figure 3b), which indicates that the pore diameter of the mesopores produced without organic additives is nonuniform. For A-CD and A-poly, one single peak with a maximum at 1.6 nm is observed, which is indicative of the wormhole-like mesoporosity observed in the TEM images of the "organic-additive-assisted" samples; this is a result of the organized aggregation of the titanium phosphonate nanoparticles that are arranged in a fairly uniform way and partially due to both intraparticle and interparticle porosity.[25] Because the BJH method somewhat underestimates the pore size of small mesopores,[27] the NLDFT method was also applied to calculate the pore width of the synthesized materials (Figure 3c).

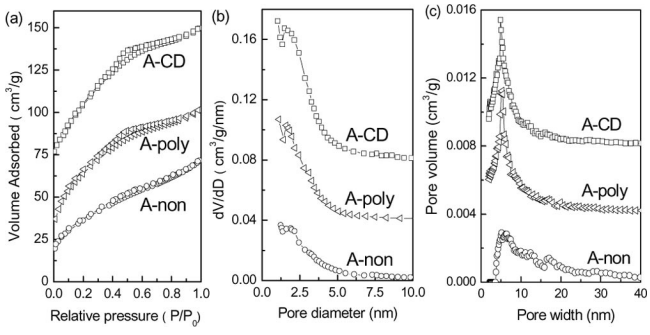


Figure 3. (a) $N_2$ adsorption–desorption isotherms and the corresponding pore size distribution curves of the synthesized samples calculated by the (b) BJH and (c) DFT methods. The volume adsorbed was shifted by 10, 5 and 0, the d*V*/d*D* value was shifted by 0.08, 0.04, and 0, and the pore volume was shifted by 0.008, 0.004, and 0 for the curves of A-CD, A-poly, and A-non, respectively.

The pore width distribution of A-non by NLDFT method is poor because of the ill-defined mesophase (Figure 2a) that occurs without the assistance of the organic additive; one peak at 4.9 and 5.0 nm for A-CD and A-poly is obtained, respectively, which is larger than the BJH pore size of about 3–4 nm. It is shown in Table 1 that the surface areas and pore volumes of the samples synthesized with organic additives (241–323 $m^2/g$, 0.16–0.22 $cm^3/g$) are both larger than those of A-non (132 $m^2/g$, 0.13 $cm^3/g$), which indicates that the autoclaving synthesis with the assistance of the diblock copolymer and β-cyclodextrin could efficiently enlarge the surface areas and pore volumes of the resultant porous titanium triphosphonates; β-cyclodextrin is more effective than $EO_{30}PO_{34}$ in improving the mesoporosity. Thus, the addition of organic additive $EO_{30}PO_{34}$ or β-cyclodextrin during the preparation process makes an obvious difference to the pore structure and the porosity of the synthesized meso-/macroporous titanium phosphonates.

The XRD patterns of the synthesized samples show broad diffraction peaks in the range $2\theta$ = 15–40° (Figure S1 in the Supporting Information), which implies that all the samples regardless of whether they are synthesized with or without $EO_{30}PO_{34}$ or β-cyclodextrin possess amorphous framework walls made up of titanium phosphonates and no crystalline titanium phosphate or $TiO_2$ phases appear. The FTIR spectra of the synthesized samples (Figure S2 in the Supporting Information) show a strong broad band at 3420 $cm^{-1}$ and a sharp band at 1630 $cm^{-1}$, which correspond to the surface-adsorbed water and hydroxy groups.[27] The bands at 1150 $cm^{-1}$ and 1050 $cm^{-1}$ are assigned to the P–$CH_2$N= groups and to the P–O···Ti stretching vibrations, respectively.[36] The band at 1324 $cm^{-1}$ could be attributed to the C–N stretching vibration, while the small band at 1437 $cm^{-1}$ arises from P–C stretching vibrations.[37] No bands at 930 $cm^{-1}$ assigned to P–OH stretching vibrations are observed, which implies extensive condensation and coordination of the phosphoryl oxygen atoms with the titanium atoms, which leads to mainly bidentate phosphonate units.

The $^{31}P$ and $^{13}C$ MAS NMR spectra of A-non are shown in Figure 4 (these are taken to be representative). The $^{31}P$ MAS NMR spectrum of A-non shows a broad signal around 13.5 ppm, which is in the area characteristic of phosphonates.[38] The broadening of the resonance signal is due to the disordered or low-crystalline nature of the solids. This signal has similar chemical shifts found for $PhP(OTi)_3$ units in molecular oxophosphonato titanium clusters of phenylphosphonate–$TiO_2$ hybrids[28,29] and for diphosphonate groups (≡P–$CH_2$–P≡) in mesoporous aluminum phosphonates.[14–16]

Table 1. Summary of the physicochemical properties and adsorption capacities of the synthesized samples.

| Sample | $S_{BET}$ ($m^2/g$)[a] | $D_{BJH-ads}$ (nm)[b] | $D_{NLDFT}$ (nm)[c] | $D_{ave}$ (nm)[d] | $V_{pore}$ ($cm^3/g$)[e] | $CO_2$ capture (mmol/g)[f] | $K_d$ (mL/g) | | |
|---|---|---|---|---|---|---|---|---|---|
| | | | | | | | $Pb^{2+}$ | $Cu^{2+}$ | $Cd^{2+}$ |
| A-non | 132 | 1.8 | 5.6 | 3.5 | 0.13 | 0.45 | 689–977 | 1397–3516 | 5058–9929 |
| A-poly | 241 | 1.6 | 5.0 | 2.6 | 0.16 | 0.56 | 914–1096 | 1730–4201 | 5850–11420 |
| A-CD | 323 | 1.6 | 4.9 | 2.5 | 0.22 | 0.60 | 1198–1259 | 2034–4531 | 6394–13328 |

[a] BET surface area calculated from the linear part of the BET plot. [b] Estimated by using the adsorption branch of the isotherms by the BJH method. [c] Pore diameters calculated by the NLDFT method. [d] Average pore size (4*V*/*A*). [e] Single point total pore volume of pores at $P/P_0$ = 0.98. [f] TGA records of $CO_2$ adsorption capacity after 60 min of flow purge at 40 °C.

  

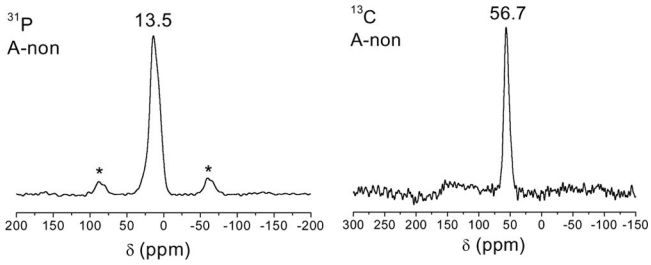


Figure 4. $^{13}C$ and $^{31}P$ MAS NMR spectra of A-non.

No sharp $^{31}P$ NMR resonance signal at –4 ppm is observed, which indicates that a layered titanium phosphonate phase[28] is not present in the synthesized hierarchically porous materials, which is further supported by TEM and IR spectroscopy. The $^{13}C$ MAS NMR spectrum shows a major signal at $\delta$ = 56.7 ppm for A-non, which corresponds to the carbon atoms in the nitrilomethylenephosphonate groups. These all suggest that no phase separation takes place during the preparation of the hybrid samples, and organophosphorus coupling groups are dispersed homogeneously within the titanium phosphonate network.[26–29]

ICP emission spectroscopy was employed to analyze the chemical composition of the resultant solids. The results show 6.45 (A-non), 6.42 (A-poly), and 6.37% (A-CD) of Ti and 8.54 (A-non), 8.50 (A-poly), and 8.42% (A-CD) of P in mass, with a P/Ti molar ratio of about 2:1. In combination with C, H and N conventional elemental analysis, all the samples synthesized with or without the assistance of $EO_{30}PO_{34}$ or β-cyclodextrin could be formulated as $Ti(C_3H_6O_9NP_3)_{0.67}{\cdot}xH_2O$ [alternatively expressed as $Ti(ATMP)_{0.67}{\cdot}xH_2O$]. By utilizing the TG-DSC analysis, the $H_2O$ molecules adsorbed on the materials and the titanium phosphonate frameworks (which are denoted in the experimental formula), could be further confirmed. Figure S3 (Supporting Information) shows the TG-DSC curves of the samples; an initial weight loss of 20.2 (A-non), 16.8 (A-poly), and 14.3% (A-CD) from room-temperature to 250 °C, accompanied by an endothermal peak at about 113 °C in the DSC curve, which may be assigned to the desorption of the adsorbed and intercalated water, was observed. The weight losses of 5.2 (A-non), 7.3 (A-poly), and 8.0% (A-CD) from 250 to 560 °C and 9.3 (A-non), 6.2 (A-poly), and 3.5% (A-CD) from 560 to 900 °C, accompanied by two exothermic peaks at 320 and 780 °C, can be attributed to the decomposition of the organic moiety in the hybrid framework and coke combustion. The TGA-DSC curves of A-poly and A-CD are similar to that of A-non, and no obvious decomposition of the organic additives was detected, which indicates that $EO_{30}PO_{34}$ and β-cyclodextrin could be removed completely by extraction of ethanol.

### Heavy Metal Ion and $CO_2$ Adsorption

Heavy metal ions, especially mercury and lead, are highly toxic environmental pollutants. A series of silica-based mesoporous organic–inorganic hybrid materials have recently been developed for removal of heavy metal ions from waste streams,[39,40] where the organic functionalities in these adsorbents typically serve to form complexes with heavy metal ions through acid–base reactions and the solid support allows easy removal of the loaded adsorbent from the liquid waste.[41] Thiols, thiourea, and amines have been used as metal-ion binding motifs for the efficient removal of toxic heavy metals such as $Hg^{II}$, $Cu^{II}$, and $Cd^{II}$.[39–42]

The synthesized meso-/macroporous titanium phosphonate materials contain organic functional groups in the framework, which can interact with the heavy metal ions. Their performance in heavy metal ion adsorption was thus studied, and the results are summarized in Figure 5. It can be seen that the percentage metal ions ($Cd^{II}$, $Cu^{II}$, and $Pb^{II}$ ions) removed by the hybrid materials is higher for all metal ions than those by pure $TiO_2$ with a high surface area (245 $m^2/g$). This proves that the observed ion concentration change is indeed attributed to the complexation reactions between the metal ions and the grafted ligands inside the hybrid framework rather than to the surface area and porous structure. Adsorption efficiency of these adsorbents follows this sequence: A-CD > A-poly > A-non. The "organic-additive-assisted" samples achieved higher adsorption capacities, probably because of the enlarged surface area and pore volume (Table 1), which afford extra binding sites for heavy metal ions.

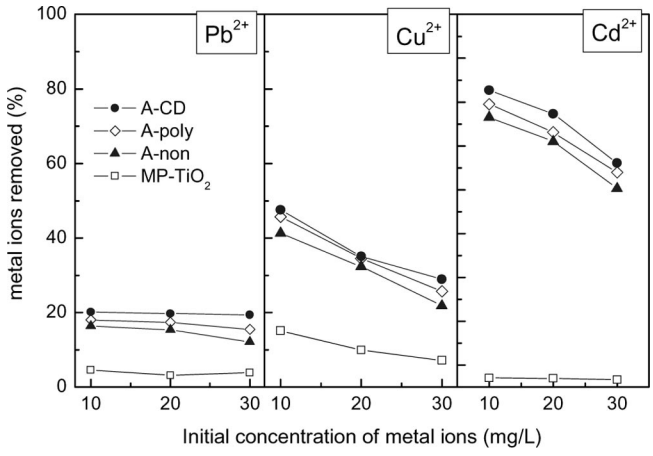


Figure 5. Percentage metal ions removed by the synthesized samples, together with MP-$TiO_2$ as reference.

Notably, the tendency for different initial concentrations of metal ions was similar for each sample, that is, the adsorption efficiencies increase with the decrease in the initial concentrations of metal ions, which clearly demonstrates that the samples essentially tend to a high loading capacity at low metal ion concentrations. Relative to the adsorption of $Pb^{II}$ and $Cu^{II}$, a significant higher binding ability for $Cd^{II}$ with removal percentages of up to 66.51, 69.55, and 72.72% was observed for A-non, A-poly, and A-CD, respectively, while a removal percentage of only 7.08% for MP-$TiO_2$ was confirmed even when the initial concentration of $Cd^{II}$ was 10 mg/L. This demonstrates the remarkable selectivity of the synthesized adsorbents for $Cd^{2+}$. This is really of great significance since the previously reported

  

organic-functionalized mesoporous silicas exhibited very weak complexation affinity for $Cd^{2+}$.[43] A competitive adsorption experiment was also performed by treating a mixed ionic solution containing $Pb^{II}$ (10 mg/L), $Cu^{II}$ (10 mg/L), and $Cd^{II}$ (10 mg/L) with A-CD. The adsorption capacities of 0.007 mmol/g $Pb^{II}$, 0.042 mmol/g $Cu^{II}$, and 0.065 mmol/g $Cd^{II}$ were obtained. The selective adsorption capacity of A-CD for $Cd^{II}$ is much higher than that of our previously reported hydroxyethylidene-bridged diphosphonate adsorbents (0.027 mmol/g) with a specific surface area of about 250 $m^2$/g.[29] A distinct preference of the synthesized meso-/macroporous titanium triphosphonate adsorbents for the uptake of $Cd^{2+}$ ions relative to that of $Cu^{2+}$ and $Pb^{2+}$ was proven, which indicates that the synthesized titanium phosphonate materials have an innate specificity for the adsorption of $Cd^{2+}$ over $Cu^{2+}$ and $Pb^{2+}$. The previously reported ligand-functionalized mesoporous silica with ethylenediamine groups have a distinct preference for the uptake of $Cu^{2+}$ ions over $Ni^{2+}$ and $Zn^{2+}$.[44] The thiol-functionalized mesoporous silicas exhibit a very small or no affinity for $Cd^{2+}$, $Pb^{2+}$, and $Zn^{2+}$, with the exception of $Hg^{2+}$, when independent homoionic solutions or a mixed metal solution were used.[43]

These results prove that the meso-/macroporous titanium phosphonate hybrids exhibit a unique selective affinity for binding heavy metal ions that can be important in the fields of metal ion recovery and environmental remediation. The distribution coefficient ($K_d$) was determined by using the equation[39,42] $K_d = (c_i\text{-}c_f)V_{soln}/(c_f m_{ads})$, where $c_i$ is the initial metal ion concentration, $c_f$ is the ion concentration after adsorption, $V_{soln}$ is the volume of the solution (in mL), and $m_{ads}$ is the amount of adsorbent (in g). The results are shown in Table 1. At an ion concentration of 10–30 mg/L, the $K_d$ values of the samples for $Cu^{II}$, $Cd^{II}$, and $Pb^{II}$ follow the same order as that of the adsorption efficiency: A-CD > A-poly > A-non, and the $K_d$ values for $Cd^{II}$ adsorbed onto the synthesized adsorbents are much higher than for $Cu^{II}$ and $Pb^{II}$.

In addition to the significance of studying liquid-phase adsorption for metal ions, as shown above, it is important to investigate the gas storage abilities (e.g. $H_2$ sorption and $CO_2$ capture) of materials. Carbon dioxide has drawn much attention for being one of the major greenhouse gases that lead to global warming. Hence, it is worth estimating the $CO_2$ adsorption performance of hierarchically porous titanium phosphonate materials. The adsorption studies were performed at ambient temperature and pressure to meet the broad needs of industry and private households. Figure 6 illustrates the $CO_2$ adsorption for the hybrid samples at 40 °C. The $CO_2$ adsorption capacity increased slowly and took a long time to reach equilibrium, which was different from the results reported in the literature, where $CO_2$ uptake initially was quite rapid and then began to slow after a couple of minutes, and an apparent equilibrium was established soon on the silica matrix modified by an amine.[45] The difference in the results indicates that the $CO_2$ is adsorbed on the synthesized titanium phosphonate samples by physical adsorption and that $CO_2$ and $N_2$ are adsorbed together, but when the samples are purged with $CO_2$, $N_2$ is replaced by $CO_2$ slowly. The equilibrium is therefore established over a long period. The sequence for the uptake of $CO_2$ after 60 min of purging is: A-CD (0.60 mmol/g) > A-poly (0.56 mmol/g) > A-non (0.45 mmol/g) (Table 1); the amounts captured are mostly higher than those for some pure silica adsorbents (0.52 mmol/g at 20 °C)[46] with specific surface areas up to 909 $m^2$/g. These hybrid materials have a higher $CO_2$ capacity than pure silica materials with larger surface areas. This indicates a much stronger van der Waals force between carbon dioxide and the synthesized materials than between $CO_2$ and pure silica materials, which results from the existence of phosphonate groups in the organic–inorganic network. However, in comparison with metal–organic frameworks (MOFs) with higher adsorption capacities and selectivities for $CO_2$ because of the pore size limit,[47,48] more work remains to be done for the improvement of the porosity and morphology of the present metal phosphonate materials for a better adsorption behavior. For physical adsorption, the gas uptake is related to the textural and structural properties such as specific surface area, the microarchitecture of the materials, and the interaction strength between adsorbent and adsorbate.[46] Thus, it is normal that A-poly and A-CD with higher surface areas have a larger $CO_2$ capture capacity than A-non. In addition, the micromorphology of the macrochannels has been proven to contribute to the reduced resistance to diffusion and improved mass transfer, as well as to the establishment of an adsorption/desorption equilibrium, which then leads to the improvement of the adsorption efficiency of the hybrid adsorbents.[38] This suggests the superiority for $CO_2$ uptake of hierarchically porous materials than bulk materials with similar surface areas and pore volumes.

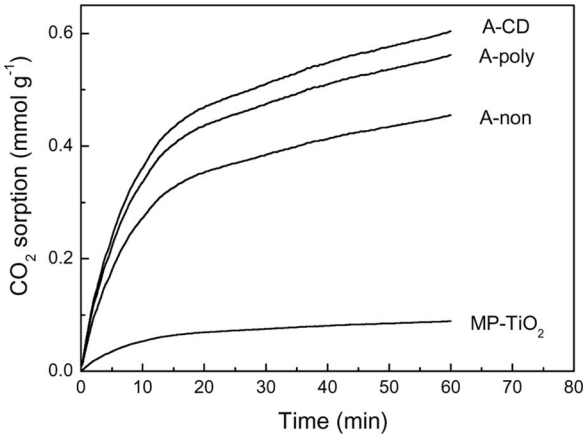


Figure 6. TGA records of $CO_2$ adsorption for the synthesized samples tested at 40 °C.

## Discussion

In the preparation of hierarchically porous titanium phosphonate materials, ATMP was used as an organophosphorus coupling molecule, and the spontaneous formation mechanism was followed in the presence/absence of organic

  

additives $EO_{30}PO_{34}$ and β-cyclodextrin. Herein, experimental conditions such as the organic additives used and the pH value of the reaction solution can greatly influence the morphology and textural property of the synthesized titanium phosphonates, as well as their adsorption behavior for metal ions and $CO_2$.

The genesis of this meso-/macroporous hierarchy in the absence of surfactant molecules corresponds to a spontaneous formation mechanism, as described by Mann et al.[23] and in our previous work.[24] The hydrolysis of tetrabutyl titanate precursors in the phosphonic acid solution would result in the rapid formation of nanometer-sized Ti-phosphonate particles, and the simultaneous generation of a large amount of butanol molecules. Self-assembly of Ti-phosphonate particles and aggregation of Ti-phosphonates along with microemulsion takes place, to produce the accessible mesopores. The hydrolysis reactions and polycondensation might produce microphase-separated domains of Ti-phosphonate-based nanoparticles and water/alcohol channels, which are the initiators of the macrochannels. Thus, a hierarchical structure of uniform macrochannels with mesoporous walls could be generated. The mesoporosity of A-non without the assistance of an additive is poor, which can be seen by the irregular aggregation of the titanium phosphonate particles (Figure 2a). This results in the low surface area (132 $m^2/g$), small pore volume (0.13 $cm^3/g$), and relatively wide pore width distribution (Figure 3). By the addition of the diblock copolymer $EO_{30}PO_{34}$, the macroporous structure remained unchanged but wormhole-like mesopores were obtained (Figure 2b); aggregated involved much smaller nanoparticles than those of A-non. Further this resulted in a larger surface area and pore volume (241 $m^2/g$, 0.16 $cm^3/g$). β-cyclodextrin was also used as an organic additive in the preparation of the hierarchically porous titanium phosphonate materials; both the macroporous structure and the mesoporosity of the synthesized solids were altered. In the last 10 years, the self-aggregation of cyclodextrin in aqueous solution have been proved and published. Different structures of the cyclodextrin clusters have been detected depending on the cyclodextrin concentration;[33] these structures include rodlike aggregates,[49] wormlike structures,[34] and spherical aggregates.[33] Polarz et al. have reported the approach of supermolecular aggregates of nonpolar cyclodextrins in aqueous solution as templates to generate porous materials.[34] Herein, the well-structured mesopores in the sample A-CD are produced by the wormlike cyclodextrin aggregates as templates; these results were supported by the $N_2$ sorption and TEM images. Spherical pores with larger sizes of 50 nm–100 nm were found among the wormhole-like mesopores, which could be the inverse spaces of the spherical cyclodextrin aggregates.[33] The surface area and pore volume of A-CD are further enlarged to 323 $m^2 g$ and 0.22 $cm^3/g$, respectively, relative to those of A-poly; in addition, the change in the $N_2$ sorption isotherms from type II to type IV could result from the addition of organic additives. Noticeably, a hierarchy with three different pore-size lengths (mesopores, small macropores, and large macropores) is integrated into one solid body of A-CD, which is of great importance in the design of structured catalysts for one-pot reactor processes.[32]

The pH value of the reaction solution is one of the most important factors that determine the textural properties of the final products. In order to investigate the effect of acidity on the porosity of the synthesized materials, NaOH solution was used to adjust the pH of the synthesis mixture from <1 to 3, 7, and 10, and the mesoporosity of A-CD obtained at the different pH values was tested by determining the $N_2$ sorption (Figure 7). When the sample was synthesized at pH = 3, the isotherm remains type IV and is characteristic of mesoporous materials; the surface area falls sharply from 323 to 189 $m^2/g$. When the sample is synthesized in a neutral (pH = 7) or basic (pH = 10) solution, the surface areas of the resultant products are rather low (3 or 2 $m^2/g$), which indicates the complete destruction of the mesoporous structure. As a conclusion, an acidic environment is necessary for the preparation of meso-/macroporous titanium phosphonate materials with high surface areas.

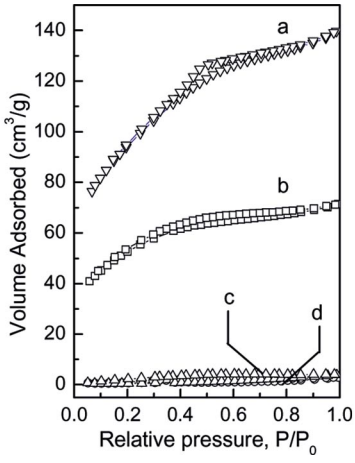


Figure 7. $N_2$ adsorption–desorption isotherms of the sample A-CD synthesized at different pH values: (a) pH < 1, (b) pH = 3, (c) pH = 7, and (d) pH = 10. The multipoint BET surface areas are 323, 189, 3 and 2 $m^2/g$ for (a)–(d), respectively.

Comparable to the silica-based mesoporous organic–inorganic hybrid materials recently developed for removal of heavy metal ions from waste streams, high adsorption of heavy metal ions was observed for the synthesized organic–inorganic hybrid titanium phosphonates. This occurs mainly because of the bridged phosphonates that contain ligands that bind metal ions. The organic motifs of the synthesized hybrid adsorbents are considered to be the dominant factor that determines the adsorption capacity. The enlarged surface area and pore volume may also contribute greatly, which can be seen from the same sequence for adsorption capacities as that for surface areas: A-CD > A-poly > A-non. All the hierarchically porous titanium phosphonate materials exhibit much higher adsorption capacities for heavy metal ions than pure mesoporous $TiO_2$, with a selective complexation affinity sequence of $Cd^{II} > Cu^{II} > Pb^{II}$, which makes them promising adsorbents for practical

  

applications including wastewater cleanup. The same tendency is observed for $CO_2$ capture, namely, the capture capacity increases with increasing surface area. The van der Waals force between $CO_2$ and the synthesized hybrid materials has been proven to be stronger than that between purely inorganic adsorbents like mesoporous silica, as a result of the existence of phosphonate groups in the organic–inorganic network.[50] Moreover, by varying the organic additives in the synthesis process, the porous architectures and the adsorption abilities for metal ions and $CO_2$ of the synthesized porous titanium phosphonate materials might be rationally adjusted.

## Conclusions

Hierarchically porous amino-bridged titanium triphosphonate hybrid materials have been prepared by a simple process, and possess an amorphous phase with high loadings of organic functional groups inside the titanium phosphonate framework. The morphology of hierarchically meso-/macroporous structures was seen in the samples synthesized both with and without organic additives. $EO_{30}PO_{34}$ and β-cyclodextrin mainly contributed to the enlargement of the surface area and pore volumes and the adjustment of pore hierarchy. The intraframework organic functional groups can act as binding sites for heavy metal ion adsorption, and high adsorption capacities for $Cd^{II}$, $Cu^{II}$ and $Pb^{II}$ were demonstrated. The strong van der Waals force between the synthesized materials and $CO_2$ has been proven, which results from the existence of phosphonate groups in the organic–inorganic network, which leads to the large capture capacity for $CO_2$.

## Experimental Section

**Material Preparation:** Amino tri(methylene phosphonic acid) (ATMP) was received from Henan Qingyuan Chemical Co. and used as organophosphorus coupling molecules. Tetrabutyl titanate (Kermel, A.R.) was the inorganic source. Nonionic diblock copolymer $EO_{30}PO_{34}$ (Nanjing Well Chemical Co., Ltd.) and β-cyclodextrin [β-CD: $(C_6H_{10}O_5)_7$, Kermel, A.R.] were used as the organic additives. All chemicals were used as received without further purification. In a typical synthesis procedure, ATMP (2.5 mmol) was added to a mixed solution of deionised water (30 mL) and ethanol (15 mL) in the presence of $EO_{30}PO_{34}$ or β-CD (0.1 mmol) whilst stirring (pH < 1), followed by dropwise addition of tetrabutyl titanate (5 mmol). After stirring for a further 24 h, the obtained mixture was sealed in a Teflon-lined autoclave and aged statically at 80 °C for 24 h. The product was filtered, washed with water, and dried at 110 °C. Removal of the organic additives was accomplished by extraction with ethanol for 96 h, and about 0.92 g of flaxen powder could be obtained. The samples are denoted as A-poly or A-CD, respectively. As a comparison, samples were prepared by the same procedure without organic additives, denoted as A-non, and mesoporous pure $TiO_2$ was also synthesized without any phosphonic acid addition, which is denoted as MP-$TiO_2$ (surface area: 245 $m^2/g$).

**Characterization:** Scanning electron microscopy (SEM) and transmission electron microscopy (TEM) were carried out with a Shimadzu SS-550 microscope at 15 kV and a Philips Tecnai G20 microscope at 200 kV, respectively. $N_2$ adsorption–desorption isotherms were recorded with a Quantachrome NOVA 2000e sorption analyzer at liquid nitrogen temperature (77 K). The samples were degassed at 150 °C overnight prior to the measurement. The surface area was obtained by the Brunauer–Emmett–Teller (BET) method, and the pore size distribution was calculated from the adsorption branch of the isotherms by the Barret–Joyner–Halenda (BJH) model and by non-local density functional theory (NLDFT). Fourier transform infrared (FTIR) spectra were measured with a Bruker VECTOR 22 spectrometer with the KBr pellet technique, and the ranges for spectrograms were 4000–400 $cm^{-1}$. X-ray diffraction (XRD) patterns were recorded on a Rigaku D/max-2500 diffractometer with Cu-$K_\alpha$ radiation operating at 40 kV and 100 mA. Thermogravimetry (TG) and differential scanning calorimetry (DSC) were performed by using a TA SDT Q600 instrument at a heating rate of 5°/min with α-$Al_2O_3$ as the reference. The chemical compositions of Ti and P were analyzed by inductively coupled plasma (ICP) emission spectroscopy on a Thermo Jarrell-Ash ICP-9000 (N+M) spectrometer, and C, N and H were analyzed on a Vario-EL elemental analyzer. Solid-state $^{31}P$ and $^{13}C$ magic angle spinning (MAS) nuclear magnetic resonance (NMR) spectra were recorded on a Varian Unity plus-400 spectrometer at spinning rates of 12 and 6 kHz and resonance frequencies of 161.9 and 100.5 MHz with recycle time of 5 and 3 s, and the chemical shifts were referenced to $H_3PO_4$ (85% in water) and tetramethylsilane (TMS), respectively.

**Heavy Metal Ion Adsorption:** The potential of the synthesized materials for $Cu^{II}$, $Cd^{II}$, and $Pb^{II}$ adsorption was tested as follows: the adsorbents (0.01 g) were added to homoionic solutions (50 mL) containing different concentrations (10, 20, 30 mg/L) of $Cu(NO_3)_2$, $Cd(NO_3)_2$, or $Pb(NO_3)_2$. After stirring for 8 h to access the adsorption–desorption balance, the mixtures were filtered, and the residual metal ion concentrations in the filtrates were analyzed by graphite furnace atomic absorption spectroscopy (AAS). The adsorption capacities of the adsorbent were then determined from the concentration difference measured between the filtrates and the initial metal ion solutions.

**$CO_2$ Adsorption:** $CO_2$ adsorption was characterized by simultaneous DSC-TGA analysis by using a TA SDT Q600 instrument under ambient pressure (1.0 atm). The samples were first activated by heating to 150 °C under a $N_2$ flow to remove the adsorbed moisture, ethanol and gases, and then cooled to 30 °C in a $N_2$ flow. During the sorption experiments, the samples were purged with $CO_2$ (20 $cm^3$/min) at 40 °C for 60 min. Upon introduction of the gas, a weight gain was observed resulting from $CO_2$ physical absorption on the sample surface. Desorption of $CO_2$ was performed by purging with $N_2$ (100 $cm^3$/min) for 180 min.

**Supporting Information** (see footnote on the first page of this article): XRD patterns, FTIR spectra, and TG-DSC profiles of A-non, A-poly, and A-CD are presented.

## Acknowledgments

This work was supported by the National Natural Science Foundation of China (No. 20973096 and 20673060), the National Basic Research Program of China (No. 2009CB623502), the Specialized Research Fund for the Doctoral Program of Higher Education (20070055014), the Natural Science Foundation of Tianjin (08JCZDJC21500), the Supporting Program for New Century Excellent Talents (NCET-06-0215), and Nankai University.

  

[1] R. Vivani, F. Costantino, U. Costantino, M. Nocchetti, *Inorg. Chem.* **2006**, *45*, 2388–2390.
[2] L. L. Gao, S. Y. Song, J. F. Ma, J. Yang, *Cryst. Growth Des.* **2007**, *7*, 895–899.
[3] K. Maeda, *Micropor. Mesopor. Mater.* **2004**, *73*, 47–55.
[4] P. H. Mutin, G. Guerrero, A. Vioux, *J. Mater. Chem.* **2005**, *15*, 3761–3768.
[5] A. Clearfield, Z. Wang, *J. Chem. Soc., Dalton Trans.* **2002**, 2937–2947.
[6] A. Clearfield, *Chem. Mater.* **1998**, *10*, 2801–2810.
[7] Z. Wang, J. M. Heising, A. Clearfield, *J. Am. Chem. Soc.* **2003**, *125*, 10375–10383.
[8] G. Alberti, F. Marmottini, R. Vivani, P. Zappelli, *J. Porous Mater.* **1998**, *5*, 221–225.
[9] G. Alberti, U. Costantino, F. Marmottini, R. Vivani, P. Zappelli, *Angew. Chem. Int. Ed. Engl.* **1993**, *32*, 1357–1399.
[10] J. Bideau, C. Le Payen, P. Palvadeau, B. Bujoli, *Inorg. Chem.* **1994**, *33*, 4885–4890.
[11] A. Distler, S. C. Sevov, *Chem. Commun.* **1998**, 959–960.
[12] N. Ren, Y. Tang, Y. Wang, S. Hu, A. Dong, W. Hua, Y. Yue, J. Shen, *Chem. Lett.* **2002**, 1036–1037.
[13] X. Shi, J. Yang, Q. Yang, *Eur. J. Inorg. Chem.* **2006**, 1936–1939.
[14] T. Kimura, *Chem. Mater.* **2003**, *15*, 3742–3744.
[15] T. Kimura, *Chem. Mater.* **2005**, *17*, 337–344.
[16] T. Kimura, *Chem. Mater.* **2005**, *17*, 5521–5528.
[17] J. El Haskouri, C. Guillem, J. Latorre, A. Beltrán, D. Beltrán, P. Amorós, *Chem. Mater.* **2004**, *16*, 4359–4372.
[18] J. El Haskouri, C. Guillem, J. Latorre, A. Beltrán, D. Beltrán, P. Amorós, *Eur. J. Inorg. Chem.* **2004**, *9*, 1804–1807.
[19] T. Y. Ma, Z. Y. Yuan, *Chem. Commun.* **2010**, *46*, 2325–2327.
[20] T. Y. Ma, X. J. Zhang, G. S. Shao, J. L. Cao, Z. Y. Yuan, *J. Phys. Chem. C* **2008**, *112*, 3090–3096.
[21] Z. Y. Yuan, B. L. Su, *J. Mater. Chem.* **2006**, *16*, 663–677.
[22] Z. Y. Yuan, A. Vantomme, A. Léonard, B. L. Su, *Chem. Commun.* **2003**, 1558–1559.
[23] A. Collins, D. Carriazo, S. A. Davis, S. Mann, *Chem. Commun.* **2004**, 568–569.
[24] Z. Y. Yuan, T. Z. Ren, A. Azioune, J. J. Pireaux, B. L. Su, *Chem. Mater.* **2006**, *18*, 1753–1767.
[25] G. S. Shao, X. J. Zhang, Z. Y. Yuan, *Appl. Catal. B* **2008**, *82*, 208–218.
[26] X. J. Zhang, T. Y. Ma, Z. Y. Yuan, *Chem. Lett.* **2008**, *37*, 746–747.
[27] T. Y. Ma, X. J. Zhang, Z. Y. Yuan, *Microporous Mesoporous Mater.* **2009**, *123*, 234–242.
[28] X. J. Zhang, T. Y. Ma, Z. Y. Yuan, *J. Mater. Chem.* **2008**, *18*, 2003–2010.
[29] X. J. Zhang, T. Y. Ma, Z. Y. Yuan, *Eur. J. Inorg. Chem.* **2008**, 2721–2726.
[30] W. Deng, M. W. Toepke, B. H. Shanks, *Adv. Funct. Mater.* **2003**, *13*, 61–65.
[31] T. Z. Ren, Z. Y. Yuan, B. L. Su, *Chem. Commun.* **2004**, 2730–2731.
[32] T. Z. Ren, Z. Y. Yuan, A. Azioune, J. J. Pireaux, B. L. Su, *Langmuir* **2006**, *22*, 3886–3894.
[33] M. Bonini, S. Rossi, G. Karlsson, M. Almgren, P. L. Nostro, P. Baglioni, *Langmuir* **2006**, *22*, 1478–1484.
[34] S. Polarz, B. Smarsly, L. Bronstein, M. Antonietti, *Angew. Chem. Int. Ed.* **2001**, *40*, 4417–4421.
[35] M. Kruk, M. Jaroniec, *Chem. Mater.* **2001**, *13*, 3169–3183.
[36] G. Guerrero, P. H. Mutin, A. Vioux, *Chem. Mater.* **2001**, *13*, 4367–4373.
[37] E. Jaimez, G. B. Hix, R. C. Slade, *Solid State Ionics* **1997**, *97*, 195–201.
[38] T. Y. Ma, X. J. Zhang, Z. Y. Yuan, *J. Phys. Chem. C* **2009**, *113*, 12854–12862.
[39] S. Dai, M. C. Burleigh, Y. Shin, C. C. Morrow, C. E. Barnes, Z. Xue, *Angew. Chem. Int. Ed.* **1999**, *38*, 1235–1239.
[40] A. M. Liu, K. Hidajat, S. Kawi, D. Y. Zhao, *Chem. Commun.* **2000**, 1145–1146.
[41] R. C. Schroden, M. Al-Daous, S. Sokolov, B. J. Melde, J. C. Lytle, A. Stein, M. C. Caubajo, J. T. Fernández, E. E. Rodríguez, *J. Mater. Chem.* **2002**, *12*, 3261–3267.
[42] S. Dai, M. C. Burleigh, Y. H. Ju, *J. Am. Chem. Soc.* **2000**, *122*, 992–993.
[43] J. Brown, L. Mercier, T. J. Pinnavaia, *Chem. Commun.* **1999**, *1*, 69–70.
[44] K, Z. Hossain, L. Mercier, *Adv. Mater.* **2002**, *14*, 1053–1056.
[45] G. P. Knowles, J. V. Graham, S. W. Delaney, A. L. Chaffee, *Fuel Process Technol.* **2005**, *86*, 1435–1448.
[46] G. P. Knowles, S. W. Delaney, A. L. Chaffee, *Ind. Eng. Chem. Res.* **2006**, *45*, 2626–2633.
[47] B. Wang, A. P. Côté, H. Furukawa1, M. O'Keeffe, O. M. Yaghi, *Nature* **2008**, *453*, 207–212.
[48] P. Kanoo, K. L. Gurunatha, T. K. Maji, *J. Mater. Chem.* **2010**, *20*, 1322–1331.
[49] A. W. Coleman, I. Nicolis, N. Keller, J. P. Dalbiez, *J. Inclusion Phenom. Mol. Recognit. Chem.* **1992**, *13*, 139–143.
[50] T. Y. Ma, X. Z. Lin, Z. Y. Yuan, *New J. Chem.* **2010**, doi:10.1039/B9NJ00775J.

Received: February 20, 2010
Published Online: May 11, 2010

  